

Constraints on Cosmological Anisotropy out to $z = 1$ from Supernovae Ia

Tsafrir S. Kolatt¹ and Ofer Lahav^{2,1}

¹ *Racah Institute of Physics, The Hebrew University, Jerusalem 91904, Israel*

² *Institute of Astronomy, Madingley Rd., CB3 0HA, Cambridge, UK*

31 October 2018

ABSTRACT

A combined sample of 79 high and low redshift supernovae Ia (SNe) is used to set constraints on the degree of anisotropy in the Universe out to $z \simeq 1$. First we derive the global most probable values of matter density Ω_M , the cosmological constant Ω_Λ , and the Hubble constant H_0 , and find them to be consistent with the published results from the two data sets of Riess et al. 1998 (R98) and Perlmutter et al. 1999 (P99). We then examine the Hubble diagram (HD, i.e., the luminosity-redshift relation) in different directions on the sky by utilising spherical harmonic expansion. In particular, via the analysis of the dipole anisotropy, we divide the sky into the two hemispheres that yield the most discrepant of the three cosmological parameters, and the scatter χ_{HD}^2 in each case. The most discrepant values roughly move along the locus $-4\Omega_M + 3\Omega_\Lambda = 1$ (cf. P99), but by no more than $\Delta \approx 2.5$ along this line. For a perfect FRW universe, Monte Carlo realizations that mimic the current set of SNe yield values higher than the measured Δ in $\sim 1/5$ of the cases. We discuss implications for the validity of the Cosmological Principle, and possible calibration problems in the SNe data sets.

Key words: cosmology: miscellaneous – cosmology: observations – cosmology: theory – supernovae:general

1 INTRODUCTION

The validity of the Cosmological Principle and the isotropy it implies gained much credibility in recent years. The small fluctuations in the CMB ($\Delta T/T \sim 10^{-5}$ on angular scale $\sim 10^\circ$) provide the strongest evidence that the universe can be well approximated by the FRW metric on scales larger than $\sim 1000 h^{-1}$ Mpc (e.g., Peebles 1993; Wu, Lahav, & Rees 1999)

On smaller scales ($\sim 100 h^{-1}$ Mpc) bulk flows of the order $v/c \sim 10^{-3}$ indicate that this isotropy breaks down. This is also manifested by significant correlation functions of galaxies and clusters on large scales, and structures like the Supergalactic Plane and the Great Attractor. The transition scale to isotropy and homogeneity is still poorly known, and so is the convergence of the acceleration vector of the Local Group with respect to the CMB. It is therefore important to quantify the degree of homogeneity and isotropy as function of scale. Traditionally this was done by searching for anisotropy in the distribution of radio sources and background radiations (Nan & Cai 1996; Evans 1992; Webster). Several new methods have been suggested to test isotropy and homogeneity on redshift scales of $z \approx 0.1 - 5$, such as measurements of *in situ* CMB temperature (Songaila et al.

1994), the derivation of an independent rest frame from multiple image lens systems (Kochanek, Kolatt, & Bartelmann 1996), and Faraday rotation signature due to anisotropic magnetic field (Kronberg 1976; Vallée 1990; Nodland & Ralston 1997).

The recent use of SNe as distance indicators (Phillips 1993; Perlmutter et al. 1995; Riess, Press, & Kirshner 1996) opened a new opportunity for accurate measurements of anisotropy on cosmological scales that previously have not been accessible. So far the SNe have been used in order to constrain the Hubble constant H_0 from a nearby sample and combinations of the matter density Ω_M and the cosmological constant Ω_Λ utilizing SNe at moderate ($\gtrsim 0.3$) and high (~ 1) redshifts. In the future, SNe samples over a wider redshift range will provide separate estimates for the two parameters. It is important to establish the ‘universality’ of the measurements of cosmological parameters from SN, as they are commonly used in joint analysis with other probes such as the CMB, cluster abundance and peculiar velocities (Efstathiou 1999; Efstathiou et al. 1999; Bridle et al. 1999; Bridle et al. ; Tegmark 1999).

Assuming a FRW cosmology, a forth measure can be deduced from the ‘Hubble diagram’ (HD; i.e., the luminosity – redshift relation), the χ_{HD}^2 measure for the best fit model.

For a perfect distance indicator this measure indicates deviations of the local potential (i.e., at the location of the SN) from a pure FRW geometry. However, in the real universe the deviations can also be due to other sources:

- Intrinsic (astrophysical) scatter in the SN luminosity-light curve relation.
- Scatter due to the location of the SN within the host galaxy & the galaxy type.
- Scatter due to dust absorption in the host galaxy, in the intergalactic medium and in our Galaxy.
- Gravitational lensing along the l.o.s. to the SN (e.g., an overdensity along the l.o.s. will enhance the apparent luminosity of a SN).

Here we explicitly assume that there is no evolution with redshift in the luminosity-light curve relation. Fortunately, most of the abovementioned effects are on the scale of the host galaxy, so with large enough sample they would be averaged out in the calculation of large scale anisotropies. On the other hand, one should worry about ‘anisotropies’ which are simply due to poor matching of different data sets that sample different portions of the sky, or large angular effects due to Galactic extinction.

We also note that some of these effects above might be correlated with other measurements, e.g. if the scatter χ^2_{HD} detected in SN Hubble diagram is affected by fluctuations in the potential, then it would be correlated with Integrated SW (or Rees-Schiama) effect in the CMB fluctuations.

The outline of this paper is as follows, in §2 we present the unified data set we will be using for the isotropy analysis. The results for cosmological parameters from the entire sample are presented in §3, the anisotropy measurement is discussed in §4, and put in a probabilistic context in §5. We conclude our results in §6.

2 THE UNIFIED DATA SET

An ideal data set of SNe for the goals we have put forward in the introduction would be a whole-sky homogeneous coverage at various redshifts of SNe. Since such an optimal set does not exist, the closest data set would be the amalgamation of the two existing, published data sets.

We unify the samples of the Supernova Cosmology Project (SCP) (Perlmutter et al. 1999) and that of the High-z Supernova search team (HZS) (Riess et al. 1998). These include also the data from low redshift of the Calán-Tololo survey (Hamuy et al. 1996). The two groups have different strategy and different nomenclature for the minimization problem by which the cosmological parameters are derived. We have brought the SCP data to comply with the language of the HZS team

For each SNe we list its (i) cz in the CMB frame, (ii) the distance modulus $\mu = m_B^{eff} - M_B^{fiducial}$, (iii) errors for these two quantities, (iv) Galactic l and b . For the SCP data the fiducial magnitude, $M_B^{fiducial}$ (cf. P99), is obtained by comparison of the 18 overlapping low redshift SNe as analysed by the two groups, and equating the distance modulus of R98 (table 10) to m_B^{corr} of P99 (table 2). This procedure is repeated twice, since Riess et al. provide two ways to calculate the distance moduli, “Multi Light Curve Shapes” (LCS) and “Template”. Errors are taken from the tables and a least

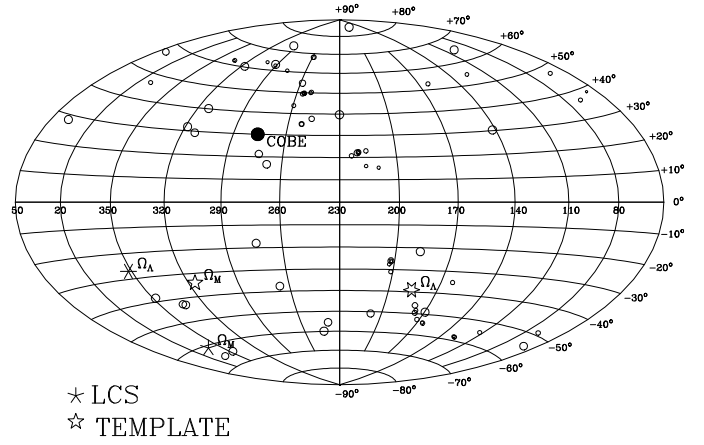


Figure 1. The sky distribution in Galactic coordinates of the 79 SNe composing the unified sample. The point size is proportional to $(1+z)^{-1}$ of the SNe. Also shown are the (positive) directions that maximize the Ω_M and Ω_Λ dipoles using the two methods (cf. §4), and the CMB dipole direction in the Local Group rest-frame as measured by COBE.

square minimization is performed in order to obtain the two best fit values of $M_B^{fiducial}$ of P99 (and to recover the Hubble constant dependence they omitted in their calculation). The two values are $M_B^{fiducial} + 5 \log H_0 = -19.322, -19.453$ with $\chi^2/d.o.f$ of 0.952 and 0.763 for the LCS method and the TEMPLATE method respectively. The value of $M_B^{fiducial}$ is degenerated with H_0 , so different H_0 calibrations in the two samples get “absorbed” in the value for $M_B^{fiducial}$. The unified sample consists of 79 SNe altogether, after the exclusion of 6 SNe from P99 (taking their “model C” version) and including the snap-shot survey from R98 along with 1997ck. Figure 1 shows the SNe distribution in Galactic coordinates.

The sky coverage is clearly inhomogeneous: the SNe deficiency near the Galactic plane is evident and the clustering of a few of the observed SNe due to the detection procedure is clear.

3 COSMOLOGICAL PARAMETERS FROM THE UNIFIED SAMPLE

We follow the statistical analysis as described in R98 and obtain best values for H_0 and probability contours in the $(\Omega_M, \Omega_\Lambda)$ plane after integration (i.e. marginalization) over all H_0 values and taking into account only physical regions in that plane.

P99 include the error due to redshift measurements and peculiar velocities in their magnitude errors, for R98 we followed their procedure, set $\sigma_v = 200 \text{ km s}^{-1}$ for SNe of $z < 0.5$ and $\sigma_v = 2500 \text{ km s}^{-1}$ for SNe with $z \geq 0.5$, and translated to the distance modulus, μ , units according to the assumed cosmological model in the likelihood function. Figure 2 show the results of the likelihood analysis. The maxima of the likelihood functions are obtained for $(\Omega_M, \Omega_\Lambda)$ values of (0.40, 0.82) and (0.66, 1.36) for the LCS and TEMPLATE method respectively. The contour lines correspond to the 68.3%, 95.4%, and 99.7% confidence levels.

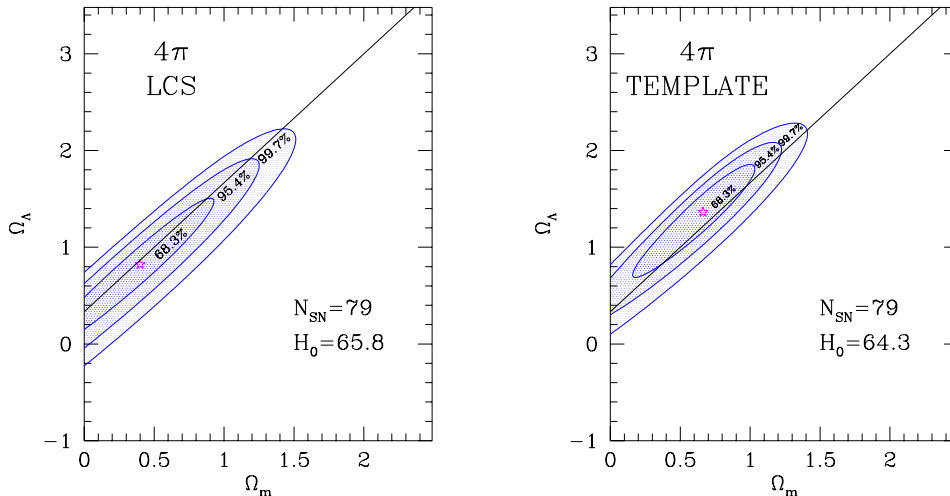


Figure 2. Confidence regions drawn from 79 SNe of the unified sample (see text), using the LCS method (left) and the TEMPLATE method (right). The best-fit parameters are marked by a star and the quoted best-fit line from P99 ($0.8\Omega_M - 0.6\Omega_\Lambda = -0.2$) is shown for reference as the diagonal line across the figure. Non-physical regions in the $(\Omega_M, \Omega_\Lambda)$ plane are excluded.

4 ANISOTROPY MEASUREMENT

The natural expansion for anisotropy detection is in spherical harmonics. The current data are too sparse to allow analysis in redshift shells.

We expand the four two-dimensional parameter ‘fields’ (for Ω_M , Ω_Λ , H_0 , and χ_{HD}^2) in spherical harmonics. If the isotropy assumption is valid we expect deviations from the average value to be due to noise, and the angular power spectrum should likewise reflect it. This is unless foreground effects alter the signal significantly.

The operational way to calculate the expansion coefficients a_{lm} is as follows.

- Build a random distribution of points (“mask”) on the sphere.
- Assign four best-fit parameters to every point based on minimization over all SNe within angular radius γ_{min} about this grid point.
- Construct the four residual fields about the global mean, i.e., $\delta_F = (F - \langle F \rangle) / \langle F \rangle$, where F is Ω_M , Ω_Λ , H_0 , or χ_{HD}^2 .
- Expand the δ_F values as obtained at each grid point in Spherical Harmonics up to $l_{max} = \pi / \gamma_{min}$, i.e.

$$\delta_F(\theta, \phi) = \sum_{l=0}^{l_{max}} \sum_{m=-l}^{m=+l} a_l^m Y_l^m. \quad (1)$$

In order to include more than 2 SNe in each smoothing bin (at least two-parameter fit) we obtain $\gamma \simeq 25^\circ$, however the SNe are not distributed uniformly (cf. Fig. 1) and thus a minimum angular resolution of $\sim 60^\circ$ is imposed. That means that for a whole sky coverage the highest significant multipole, l , is $l = 3$. There are, though regions that are more densely covered by SNe data and therefore higher multipoles can be assessed as well but at a lower signal-to-noise level.

In order to account for the Poisson noise contribution (and thus to the angular power spectrum in quadrature), we run a set of 50 random “masks” and repeat the a_{lm} calcu-

lation each time. For each set of a_{lm} the power spectrum coefficients, $C_l = (2l + 1)^{-1} \sum_{m=-l}^l |a_{lm}|^2$ are computed.

The angular power spectrum of the δ_{H_0} is an order of magnitude and more smaller than the noise level ($C_l / (2\pi) \simeq 5 \times 10^{-5}$), in both methods. Figure 3 shows the angular power spectrum, $l(l+1)C_l / (2\pi)$, for the other three fields as calculated from 50 runs with different random mask points. The straight weaker lines show the noise level in each field. The δ_Ω fields in both methods show signals that exceed the noise level for the dipole ($l = 1$) and the quadrupole ($l = 2$). Two factors contribute to the noise level, the discrete number of SNe, and the scatter in the luminosity — redshift relation. The former is common to both methods (LCS and TEMPLATE) and therefore the order of magnitude higher noise level for the δ_Ω fields in the LCS method must be due to the latter. The TEMPLATE method seems to provide smaller errors and a better match between the two data sets, as indicated by the lower χ^2 level of the fiducial magnitude calibration (cf. §2). The $\delta_{\chi_{HD}^2}$ angular power spectrum is similar in shape and magnitude in both methods, and lies an order of magnitude to a factor ~ 5 above its noise level. This may indicate there exists a true dipole (or quadrupole) in this field. From the first multipole of angular power spectrum alone, one cannot deduce what is the dipole *direction*. We therefore turn to look for the direction by other means.

We search for largest dipole in Ω_M , Ω_Λ , H_0 , and χ_{HD}^2 . This has been done in two ways : an actual search over the sky, dividing the SN population in between two hemispheres, and equivalently, by solving a maximization problem of the dipole term with respect to (θ, ϕ) using the computed a_{lm} coefficients. Both methods yield similar results. We then calculate the confidence regions for each hemisphere separately, and look for statistical consistency (overlapping contours). Each test can be applied to each one of the four parameters.

Figure 4 verify the fact that the current SNe data best constrain a linear combination of the cosmological parameters Ω_M , Ω_Λ . In all four panels the likelihood maxima move along the line (P99) $-4\Omega_M + 3\Omega_\Lambda = 1$, sometimes with

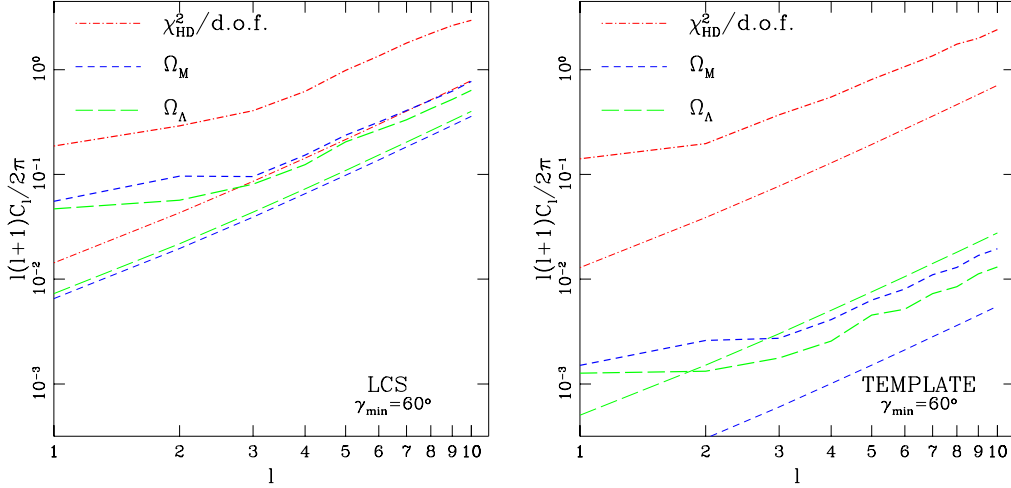


Figure 3. Angular power spectrum coefficients for the two dimensional fields: δ_{Ω_M} , δ_{Ω_Λ} , and $\delta_{\chi_{\text{HD}}^2}$ along with the noise level of each field (straight weak lines). Shown are results from the LCS method (right) and the TEMPLATE method (left).

a large distance Δ between the two maxima for the two disjoint hemispheres (quoted on the plots). In three cases the contour levels overlap significantly (see next section for quantitative evaluation). In the case of the Ω_Λ dipole, using the LCS method, there is no overlap between the 99.7% confidence levels of the two hemispheres. The discrepancy stems from the very asymmetric distribution of SNe between the two hemispheres (59 on one versus 20 on the other) and only one SN (1995at) with $z > 0.5$ in the 20 SNe sample. A small error in the distance measurement of this SN, or a systematic deviation of it from the average LCS relation may cause such a discrepancy as we demonstrate in the next section. Elimination of this SN yields a dipole which points $\sim 20^\circ$ away from the original direction, reduced Δ value of 2.39, and almost full inclusion of the 99.7% confidence contour for the larger sample (56 SNe) within the 95.4% confidence level of the remaining 22 SNe.

Note that a different “mixture” of redshift distribution to different directions may cause some directions to become more sensitive to one parameter. E.g., SNe at $z \simeq 0.4 - 0.5$ are mostly sensitive to the $\Omega_M - \Omega_\Lambda$ combination, as opposed to higher weight on Ω_M as redshift increases ($|\partial\Delta/\partial\Omega_M| > |\partial\Delta/\partial\Omega_\Lambda|$). Figure 1 includes the dipole directions (positive) of Ω in both methods. We observe no coincidence with any Galactic or CMB direction, moreover not all dipoles point to the same direction.

The dipole of the $\delta_{\chi_{\text{HD}}^2}$ field points in both methods toward $(l = 80^\circ, b = -20^\circ)$ with $\langle\chi_{\text{HD}}^2\rangle = 1.00$ (1.01) and largest difference of 0.60 (0.63) for the LCS (TEMPLATE) method. This dipole direction is suspiciously close to the Galactic plane.

One worry is that the detected signal is due to the (mis)match between the two data sets. We therefore repeated the computation for each data set separately and verified that though the noise level increases, the results as drawn from each one of the data sets are consistent with the results from the unified set both in magnitude and direction.

5 DEGREE OF ANISOTROPY

The results of the last section, regarding the spherical harmonic expansion and the various dipole magnitudes, should now be put in an expected distribution in order to draw conclusions about the degree of anisotropy.

The hypothesis we are trying to address is that the SN data do not falsify the FRW geometry as a reliable description of the $z \simeq 1$ Universe. This strategy is more efficient than addressing specific anisotropic cosmological models (C el erier 2000a; C el erier 2000b). We therefore compute the probability distribution of the dipole magnitudes within a FRW universe and confront it with the values obtained for the real Universe.

A simple two dimensional Kolmogorov-Smirnov test to falsify the hypothesis that the two contour maps come from the same underlying distribution of cosmological parameters is inadequate here. Since we have used the maximum discrepant values in order to obtain the dipole, the two sub-samples are not randomly selected and therefore can not be confronted in a KS test.

The probability distribution depends on the actual cosmological values and to a lesser extent on the power spectrum (via the scatter due to potential fluctuations). For a self consistency check, the underlying cosmology is taken to be the “best fit” cosmological model (§3), which we then sample by Monte-Carlo simulations.

To mimic accurately the SN sample, we use the same angular locations and redshift values as of the observed sample. Luminosity distances, magnitude scatter and peculiar velocities are drawn from Gaussian distributions with the appropriate observed standard deviation.

The dipole analysis is repeated for 200 mock catalogs of the SN and the maximal dipole magnitude is calculated to obtain its distribution for *the current sampled* SNe.

Table 1 shows the rejection levels of the hypothesis that the Universe up to $z \simeq 1$ can be described by a FRW metric. E.g., using the LCS method and the current sample of SNIa we expect in 19% of all cases to detect a higher Δ value for Ω_M dipole, than the observed one.

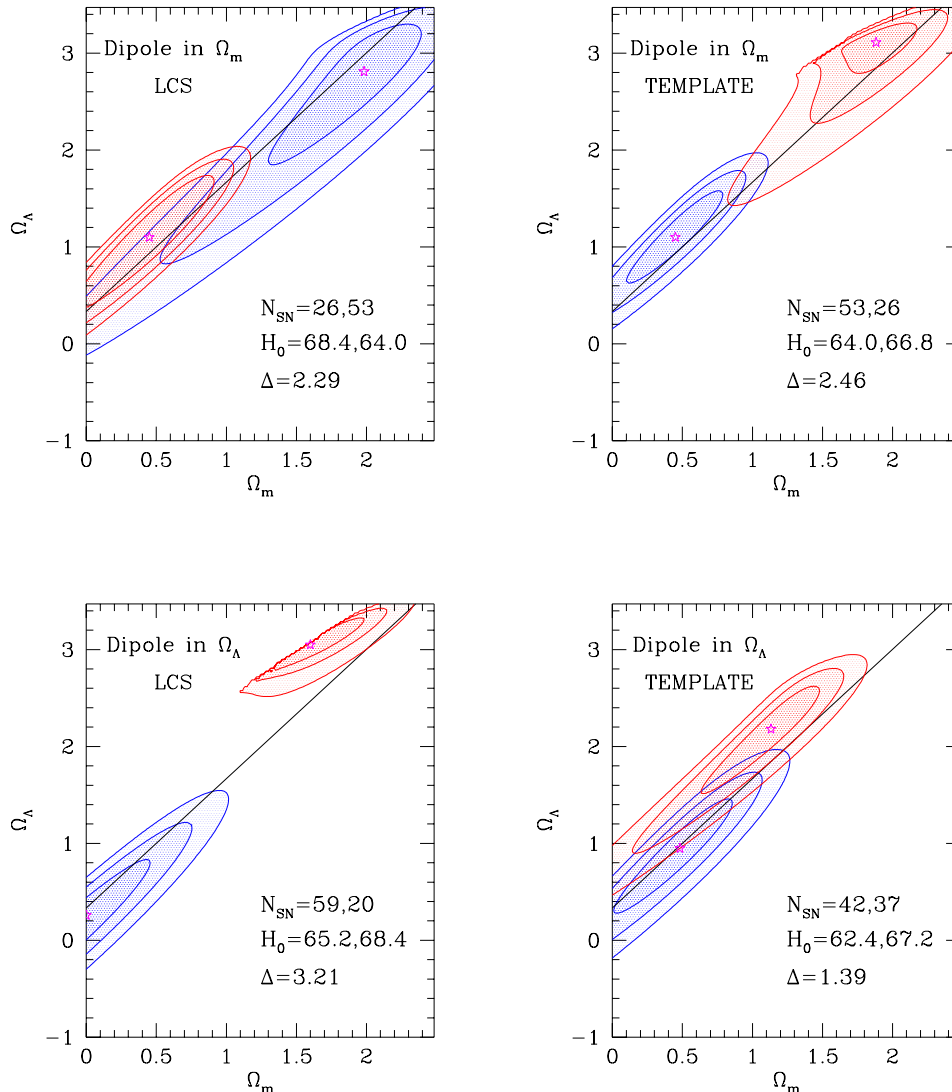


Figure 4. Confidence regions (same as Fig. 2 drawn from 79 SNe of the unified sample in two hemispheres that maximize the Ω_M dipole (up) and Ω_Λ dipole (bottom) using the LCS method (left) and the TEMPLATE method (right). Marked are the number of SNe in each hemisphere, the best-fit H_0 , and the distance between peak probabilities (Δ).

Table 1

Isotropy rejection levels using Δ		
Cosmological parameter	Method	
	LCS	TEMPLATE
H_0	33%	70%
Ω_M	81%	79%
Ω_Λ	88%	64%

6 DISCUSSION

By the exploitation of the current available SNe data we have put constraints on the rejection level of the cosmological principle validity up to $z \simeq 1$. A FRW metric is found to be an adequate description of the Universe. In $\sim 20\%$ of all realizations of such universes, the dipole signature for

anisotropy in the cosmological parameters H_0 , Ω_M and Ω_Λ exceeds the observed one.

Even though such dipole magnitudes are reasonable in the framework of the FRW model, they may be indicative of non-cosmological contributions to the angular power spectrum. In §1 we listed possible such contributions. If indeed the Universe up to $z \simeq 1$ is well represented by a FRW metric then we can exclude large coherent structures at $z \gtrsim 0.3$. Such are the structures that may lead to dipole and quadrupole signatures due to coherent gravitational lensing magnification/de-magnification and therefore the latter can be excluded as anisotropy contributors.

That leaves small scale (Galactic) foreground effects to be the most likely power contributors. The Galactic disk geometry makes the quadrupole the most significant multipole to be considered, though the solar system offset from the Galactic center may bring about a dipole contribution as well. In the current sample the quadrupole term is only

slightly larger than the noise level and does not allow any conclusive results. None of the dipole directions for Ω coincides with the Galactic plane and thus they are probably not correlated with it. Multipoles due to dust extinction may be affirmed by multiple expansion of the residual colors after extinction correction (i.e., R98 and P99 appendices).

The one case where two significantly non-overlapping confidence regions are found for two hemispheres that maximize the Ω_Λ dipole (LCS), is probably due to a single SN (1995at) for which the individual errors have been underestimated. This case is an exception since the overall χ^2 values for the HD fits are statistically acceptable. Nevertheless, this case demonstrates the hazard in the draw of conclusions based on a handful of SNe, for which the error in the error estimate is uncertain.

In general, the TEMPLATE method provides a better statistical agreement of the data with an FRW model and the current SNe data. This is seen from the magnitude match (cf. §2), tighter constraints from the combined set, smaller noise levels for all multipoles, and smaller Δ values for the Ω dipoles.

We conclude that an isotropic $z \sim 1$ universe cannot be rejected by more than a 1σ level based on the current SNe data.

ACKNOWLEDGMENTS:

This work was supported by the US-Israel Binational Science Foundation, by the Israel Science Foundation, and by grants from NASA and NSF at UCSC.

REFERENCES

- Bridle S. L., Eke V. R., Lahav O., Lasenby A. N., Hobson M. P., Cole S., Frenk C. S., Henry J. P., 1999, MNRAS, 310, 565
 C el erier M., 2000a, A&Ap, 353, 63
 C el erier M., 2000b, in "Proceedings of the XXXVth Rencontres de Moriond, "Energy Densities in the Universe", astro-ph/0006273
 Efstathiou G., 1999, MNRAS, 310, 842
 Efstathiou G., Bridle S. L., Lasenby A. N., Hobson M. P., Ellis R. S., 1999, MNRAS, 303, L47
 Evans T., 1992, Thesis Haverford Coll., PA.
 Hamuy M. et al., 1996, AJ, 112, 2408
 Kochanek C. S., Kolatt T. S., Bartelmann M., 1996, ApJ, 473, 610
 Kronberg P., 1976, in Int. Astron. Union Symp., Vol. 74, p. 367
 Nan R., Cai Z., 1996, in IAU Symp. 168: Examining the Big Bang and Diffuse Background Radiations, Vol. 168, p. 491
 Nodland B., Ralston J. P., 1997, Phys.Rev.Lett., 78, 3043
 Peebles P. J. E., 1993, Principles of Physical Cosmology. Princeton Univ. Press, Princeton, NJ
 Perlmutter S. et al., 1999, ApJ, 517, 565
 Perlmutter S. et al., 1995, ApJ, 440, L41
 Phillips M. M., 1993, ApJ, 413, L105
 Riess A. G. et al., 1998, AJ, 116, 1009
 Riess A. G., Press W. H., Kirshner R. P., 1996, ApJ, 473, 88
 Songaila A. et al., 1994, nat, 371, 43
 Tegmark M., 1999, ApJ, 514, L69
 Vall e J. P., 1990, ApJ, 360, 1